



HHS Public Access

Author manuscript

Anal Chem. Author manuscript; available in PMC 2017 April 05.

Published in final edited form as:

Anal Chem. 2016 April 5; 88(7): 3917–3925. doi:10.1021/acs.analchem.6b00100.

Quantifying the Impact of Nanoparticle Coatings and Non-uniformities on XPS Analysis: Gold/silver Core-shell Nanoparticles

Yung-Cheng Wang^a, Mark. H. Engelhard^b, Donald R. Baer^b, and David G. Castner^{a,c}

^aNational ESCA & Surface Analysis Center for Biomedical Problems, Department of Bioengineering, Box 351653, University of Washington, Seattle, WA 98195-1653 USA

^bEnvironmental Molecular Sciences Laboratory, Pacific Northwest National Laboratory, Box 999, Richland WA 99352

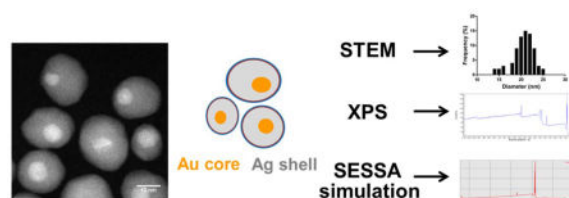
^cNational ESCA & Surface Analysis Center for Biomedical Problems, Department of Chemical Engineering, Box 351653, University of Washington, Seattle, WA 98195-1653 USA

Abstract

Spectral modeling of photoelectrons can serve as a valuable tool when combined with X-ray photoelectron spectroscopy (XPS) analysis. Herein, a new version of the NIST Simulation of Electron Spectra for Surface Analysis (SESSA 2.0) software, capable of directly simulating spherical multilayer NPs, was applied to model citrate stabilized Au/Ag-core/shell nanoparticles (NPs). The NPs were characterized using XPS and scanning transmission electron microscopy (STEM) to determine the composition and morphology of the NPs. The Au/Ag-core/shell NPs were observed to be polydispersed in size, non-spherical, and contain off-centered Au-cores. Using the average NP dimensions determined from STEM analysis, SESSA spectral modeling indicated that washed Au/Ag-core shell NPs were stabilized with a 0.8 nm layer of sodium citrate and a 0.05 nm (one wash) or 0.025nm (two wash) layer of adventitious hydrocarbon, but didn't fully account for the observed XPS signal from the Au core. This was addressed by a series of simulations and normalizations to account for contributions of NP non-sphericity and off-centered Au-cores. Both of these non-uniformities reduce the effective Ag-shell thickness, which effect the Au-core photoelectron intensity. The off-centered cores had the greatest impact for the particles in this study. When the contributions from the geometrical non-uniformities are included in the simulations, the SESSA generated elemental compositions that matched the XPS elemental compositions. This work demonstrates how spectral modeling software such as SESSA, when combined with experimental XPS and STEM measurements, advances the ability to quantitatively assess overlayer thicknesses for multilayer core-shell NPs and deal with complex, nonideal geometrical properties.

Graphical Abstract

Supporting Information: Correlation between the polydispersity, non-sphericity, and Au-core off centered effects in the Au-core/Ag-shell NPs. Comparison of Σ RMSD from experimental XPS results and SESSA simulations for one wash and two wash samples. XPS survey and high-energy resolution spectra are shown and interpreted.



Keywords

core-shell nanoparticles; nanoparticles; nanoparticle characterization; XPS; SESSA

Nanoparticles (NPs) ranging from the sizes of 1 to 100 nm are being used in many branches of science and incorporated into a wide variety of commercial products. Despite the exciting advancement in the applications of NPs, important aspects such as biocompatibility, biostability, and the environmental impact of these NPs must be well characterized for their safe and effective use.^{1, 2} Attention must also be focused on the concerns of inadequate characterization and under-reporting of data for NP used in biomedical applications.²⁻⁵ Previous studies aimed at elucidating the relationship between NPs and their physiochemical properties have concluded that synthesis method, size, shape, handling history and surface functionalization of NPs can all play important roles in determining their toxicity and circulation time in biological systems.⁶⁻⁹ Common methods used to characterize these properties of NPs include transmission electron microscopy (TEM), dynamic light scattering (DLS), UV/Vis, and Zeta potential measurements.¹⁰ Although these methods provide essential and important information about NPs, they don't provide important detailed and quantitative information about the NP surface composition or indicate possible presence of submonolayer levels of contaminants often present on NP surfaces. It is the outermost surface of nanoparticles, often coated with deliberate or accidental overlayers that directly interact with the surrounding environment. Thus, it is important to use a multi-technique approach to obtain a detailed, quantitative characterization of the surface structure and composition of NPs.

Increasingly X-ray photoelectron spectroscopy (XPS) is being used to characterize NPs³ because it can be used both to detect the presence of monolayer surface coatings and, in combination with computational modeling, thicknesses of single or multiple layers for structured particles.¹¹⁻¹⁴ Exponential sensitivity to analysis depths up to ~10 nm makes XPS a useful tool for characterizing NPs that are similar in dimension. XPS is frequently used to identify and verify the presence of functionalized chemical groups and attached-biomolecules on the NP surface through qualitative and quantitative analysis.^{1, 15-21} Combining quantitative XPS results and prior knowledge of the overall NP composition, structural properties of the NPs such as particle diameter and overlayer or multiple layer thicknesses can be determined.^{22, 23}

To date methods of determining shell thicknesses using XPS analysis assume a uniform particle shape and size. Most of these methods also assume a uniform coating thickness and some require extensive calculations.^{11, 13} Shard developed a more user friendly method for estimating shell thickness of spherical core-shell NPs²⁴ that was recently extended to

spherical core-shell-shell NPs.²⁵ For particles with additional overlayers or complex morphologies, numerical simulations of various types have been used for calculating layer thicknesses and remain the most useful approach. Earlier generations of the numerical simulations for determining the structure of complex spherical particles involved fairly complex simulations not readily amenable for routine use.¹¹

Fortunately there are now several alternative codes that enable an analyst to more routinely model XPS signals from multiple types of nanostructures. These codes provide information such as overlayer or multiple-layer thickness and can be extended to explore effects such as variations size and shape. MultiQuant,^{26, 27} Quantitative Analysis of Surfaces by Electron Spectroscopy (QUASES),^{28, 29} and Simulation of Electron Spectra for Surface Analysis (SESSA)^{33–35} are among analytical codes that can be used to quantitatively examine the impacts of nanostructure on XPS signals. QUASES can determine the composition and structure of surface nanostructures based on the analysis of peak intensity, peak shape, and the background of inelastic electrons.^{28, 29} MultiQuant focuses on the impact of particle geometry on relative signal intensities while SESSA is designed for the simulation of the entire photo- and Auger-electron spectrum from a user defined sample.^{30–32} The previous version of SESSA (Ver. 1.3) was limited to the spectral simulation of layered flat substrates and cannot be directly applied to spherical samples. However, it was successfully applied to characterize the overlayer thickness and structure of 16-mercaptohexadecanoic acid self-assembled monolayer (C16 COOH-SAM) on gold NPs by using a summation of geometrical components with flat surfaces to represent spherical particles.¹² The most recent version of SESSA (Ver. 2.0) is capable of generating XPS spectra for flat and nanostructures such as islands, spheres, and layered spheres without the need for a user to make a series of complex geometrical corrections.³² With the ability to simulate multi-layer NPs directly, SESSA can now be easily combined with experimental XPS analysis to provide direct insight into overlayer thickness and structures of NPs.³³

Although particle uniformity is a target for many synthesis processes and assumed in modeling work, such uniformity is rarely fully achieved. In this work, we used SESSA 2.0 to examine the impact of variations in size, distortions of shape, and effective coating thickness on XPS signals from Au/Ag-core/shell NPs. The particles had been stabilized by sodium citrate and were also covered, as should be expected, by a thin layer of adventitious hydrocarbon. Scanning transmission electron microscopy (STEM) analysis of a series of particles showed that the core/shell Au/Ag NPs, described previously,⁷ had a polydispersed size distribution, often had slightly non-spherical shapes, and had Au cores that were frequently off-center. The STEM measurements were used to determine average dimensions of the Au core and Ag shell as well as the distribution of deviations from that average. We then combined SESSA's new capability of directly modeling spherical NPs with the experimental XPS results to determine the thickness of the overlayers and, with additional calculations, investigated on how the variations in particle structure impacted the quantitative XPS analysis.

Results and Discussion

Nanoparticle characterization

The size and non-sphericity of the Au/Ag-core/shell NPs were determined from Image J analysis of the STEM images (Figure 1a&b). The STEM image of each NP is a 2-D projection of that particular particular NP. Since the NPs are randomly oriented, by averaging the results from a sufficient number of NPs these 2-D projections provide a good representation of the 3-D information. The NPs had a mean diameter of 20.5 ± 2.4 nm (Figure 1c) and an average non-sphericity of 1.14 ± 0.1 , as measured using the ratio of the major axis to minor axis for individual NPs (Figure 1d). The size and non-sphericity calculations were based on analysis of 76 particles. The NPs had a wide size distribution ranging from 13.8 nm to 24.8 nm and most deviated noticeably from a perfect sphere (*e.g.*, more than 60% of the particles had a major-axis / minor axis ratio larger than 1.1). Off-centered Au-cores, defined as the difference between the center of the whole particle and the center of the Au core, were also observed for most NPs.

Figure 2 shows the cross sectional schematic of the ‘ideal’ or ‘average’ Au/Ag-core shell NPs assuming they were spherical particles with the average particle size and core diameter measured from the STEM images. As purchased from the manufacturer, the Au/Ag-core shell NPs were stabilized with sodium citrate. The outermost adventitious hydrocarbon overlayer likely originates from the various steps in sample handling including air exposure during preparation prior to XPS analysis.

The mean diameter of the Au-core and the mean Ag-shell thickness measured manually from the STEM images were 7.4 ± 0.9 nm and 6.4 ± 2.3 nm. The whole particle diameter calculated using these manual measured results (20.2 nm) matches well with the particle diameter (20.5 ± 2.4 nm) determined from ImageJ’s particle analysis algorithm. Further, no correlation was observed between the polydispersity, non-sphericity, and Au-core off centered effects in the Au-core/Ag-shell NPs (see the supplementary Figure S1–S3).

XPS analysis

For comparison to SESSA we focus primarily on examination of the XPS determined atomic compositions and comparing the experimental determined values to those simulated from various models. The XPS determined atomic compositions for the one-wash and two-samples are shown in Table 1. The XPS survey and high-resolution spectra along with a more detailed interpretation of the species detected is provided in the supporting information. The XPS compositions are determined in the standard way using peak areas and sensitivity factors and assuming a flat surface and uniform elemental distribution. This information is effectively “reinterpreted” using SESSA or other modeling methods to obtain layer and coating information.

XPS results for a sample of NPs that had been deposited without washing (no-wash sample) are also included in Table 1 to highlight the importance of washing. Over time many different versions of the no-wash samples had been prepared directly from the citrate buffer solution. However, large variations in the carbon concentrations were detected, attributable to a mixture of citrate and contaminants from the solution in addition to the citrate coated

particles. An example of a results from a no-wash sample that had only the expected elements of Ag, Au, C, O and Na and a relatively low amount of carbon is shown in Table 1.

XPS analysis of three-wash samples was also done, but aggregation of the NPs made it difficult to deposit a uniform layer of NPs onto the silicon substrate, resulting in the presence of significant XPS substrate signals (e.g., Si) from all three-wash samples. Thus, because significant substrate signals were detected from all three-wash samples analyzed, no XPS results from the three-wash samples are included in Table 1. The problems encountered analyzing the no wash and three-wash samples provide yet another example of how NP handling and processing can have a significant influence on the characterization results and the necessity of documenting the history and state of the NPs analyzed.

The XPS atomic compositions of the one- and two-wash samples are the same within experimental error, although for the two-wash sample the concentrations of elements from the citrate and hydrocarbon overlayers (C, O and Na) are slightly lower and the concentrations of the elements from the metallic core (Ag and Au) are slightly higher than for the one-wash sample. The XPS atomic composition of the no-wash sample is significantly different from both the one-wash and two-wash samples, with increased signals from thicker citrate and hydrocarbon layers which result in increased attenuation of Ag and Au signals from the metallic core. The stoichiometric atomic ratio of C/O for sodium citrate is 0.86. The observed C/O ratio in the one- and two-wash samples is slightly higher (1.0), consistent with the presence of small amounts of adventitious hydrocarbon. The C/O ratio is even higher (1.4) on the no-wash sample, indicating the presence of a thicker adventitious hydrocarbon layer on this sample. Further quantification of the XPS results will be provided below.

SESSA simulations

SESSA simulations of the Au/Ag-core/shell NPs were initially based on the schematic NP presented in Figure 2. The Au-core diameter and Ag-shell thickness of the NP model were measured from STEM images. To obtain accurate thickness of the sodium citrate and adventitious carbon layers, SESSA simulations were performed for the one- and two-wash samples by varying the thickness of both layers to find the best match to the experimental XPS elemental composition. For the one- and two- wash samples, respectively, it was determined that a 0.05 nm and 0.025 nm thick adventitious hydrocarbon layers provided the best match between the SESSA determined and experimentally determined elemental composition of the NPs (Table S1). As expected from the XPS composition in Table 1, the no-wash sample had a noticeably thicker (~0.2 nm) adventitious hydrocarbon overlayer.

Figure 3 shows the SESSA results for varying the thickness of the sodium citrate layer (using fixed 0.05 and 0.025 nm thick adventitious carbon overlayers) on the one- and two-wash Au/Ag-core/shell NPs. An increase in sodium citrate layer thickness results in a decrease in the gold and silver intensities from the NP core/shell with an increase of the carbon, sodium, and oxygen intensities from sodium citrate overlayer. To quantitatively determine the appropriate sodium citrate thickness for the one-wash and two-wash sample, the sum of the root mean squared deviation (Σ RMSD) of the simulated results for each element was compared with the experimental XPS result. Smaller Σ RMSD value implies a

better match between the experimental and simulated elemental composition. Simulation using a 0.8 nm thick sodium citrate layer provided the lowest Σ RMSD and therefore the best fit with the experimental XPS results for the NPs after one wash and two wash. Table S1 shows the combined effect of varying sodium citrate and adventitious hydrocarbon layer thickness on the Σ RMSD value. Thus, the second centrifuge washing resulted in at most a slight reduction of the adventitious hydrocarbon layer thickness. In comparison the citrate layer was $\sim 2\times$ thicker (~ 1.8 nm) on the no-wash sample. For all samples, the SESSA simulated gold intensities were on average lower than the experimental gold intensity by a factor of >3 .

The underestimation of gold intensity by SESSA simulations using an “average” spherical particle is due to the actual geometrical properties of the Au/Ag-core/shell NPs shown in Figure 1 (range of sizes, non-spherical shape and offset Au cores). The wide distribution in particle sizes can potentially impact the simulation result as the ratio of surface to bulk atoms will change with particle size. However, the majority of the polydispersity for the Au-core/Ag-shell NP particle sizes was due to variations in the Ag-shell thickness due to both particle non-sphericity and deviation of the core from the particle center. As shown in Figure 2, STEM image analysis showed the mean Au-core diameter has a smaller variation (± 0.9 nm) than the variation in the Ag-shell thickness (± 2.3 nm). The polydispersity of the NPs can be described geometrically by deviations in NP non-sphericity and the off-centered position of the Au-core, as both of these quantities affect the NP’s Ag-shell thickness (distance from the Au-core surface to the particle surface) distribution. Simulations of different NP structures were used to determine the sensitivity of XPS signals to the different types of variations observed in the real nanoparticles.

Since NPs can only be simulated as perfect spheres with fixed diameter in the current version of SESSA, the contribution from non-spherical NPs with off-set cores cannot be accounted for directly with SESSA. Before accounting for the non-idealities in the simulations it is informative to see how much error is introduced by assuming a spherical shape with a centered core and a 20.5 nm diameter for the Au core plus Ag shell. Using these assumptions, the model that provides the best match between SESSA calculations and experimental XPS composition has a 11 nm Au core, 4.8 nm Ag shell, 0.8 nm citrate shell and 0.05 nm hydrocarbon overlayer. Compared to the values measured from the STEM images, this model produces a Au core diameter that is $\sim 50\%$ larger and a Ag shell thickness that is 25% smaller. Due to the size of the errors it is apparent the non-sphericity and off-centered cores of the NPs must be accounted for. Since XPS averages the composition of all nanoparticles in the sampling area one way to incorporate the effects of the off-centered Au cores is to consider a “virtual” AgAu alloy core (i.e., an alloy core with the composition and size that would result from the observed distribution of Au core positions in the nanoparticles). This can be modeled as AgAu alloy core with a lower Au composition and larger diameter than a pure Au core. Simulations done using this model determined that an alloy core with a diameter of 17 nm and a composition of 91 atomic % Ag and 9 atomic % Au would be consistent with the observed experimental XPS composition. A 17 nm core is not consistent with the STEM images, but it is consistent with the range of offsets observed in the Au core position. A common result for both ideal spheres and alloy core models is that the Ag shell thickness was significantly thinner than the value determined from STEM

imaging. So another approach was employed where both the non-spherical shape and off-center Au cores of the Au/Ag-core/shell NPs were used to provide of a range of effective Ag-shell layer thicknesses that were then modeled with SESSA. These different Ag-shell thicknesses result in different degrees of Au photoelectron attenuation. Experimentally, Au photoelectrons passing through different thicknesses of Ag-shells do not average out since Au photoelectron intensity depends exponentially on the distance traveled. Both the non-spherical properties of the Au/Ag-core shell NPs and off center cores can therefore contribute to the underestimation of gold intensity by SESSA simulations.

The degree of the off-centered Au-core was characterized quantitatively by measuring the distance between the center of the Au-core and the center of the whole Au/Ag-core shell NP (Figure 4). Off-centered Au cores were observed in most NPs, with an mean off centered distance of 2.2 ± 1.3 nm (Figure 4b). Similar to non-spherical NPs, off-centered Au-cores will lead to range of Ag-shell thicknesses and the underestimation of gold intensity by SESSA simulations.

To quantify the impact of the non-spherical NPs and off-centered Au-cores we investigated how altering the dimension of the Au-core diameter and Ag-shell thickness affected the simulated results for the one-wash and two-wash NPs (Figure 5). These axes of these plots show the “deviation” or DELTA of the effective Ag shell thickness and Au core diameters relative to those of the “average” particle. The optimal sodium citrate and adventitious hydrocarbon layer thicknesses determined from earlier simulations (Figure 3 and Table S1) were used for these simulations. The difference of gold elemental atomic % between the experimental XPS results and the SESSA simulations were plotted as a function of the delta Au and Ag dimensions. The darker blue region in the both panels of Figure 5 corresponds to specific combinations of Au and Ag dimensions that produce the best agreement between the experimental XPS results and the SESSA simulations. The red circle located near the center of figures indicates the average dimension of the Au/Ag core-shell NPs determined from the STEM images. From the previous simulations shown in Figure 3, it was determined that the average experimental STEM dimensions alone could not adequately model the actual Au/Ag-core/shell NPs as they do not account for the complex geometrical properties of the actual NPs. For both the one-wash and two-wash samples, the results in Figure 5 show that to best match the SESSA Au atomic % to the experimental Au atomic % requires the Ag-shell thickness to decrease by 2.5 nm, which is comparable to the standard deviation of the STEM determined Ag shell thickness. Note that increasing the Ag shell thickness above the average STEM dimension results in minimal changes in the Au atomic % since the simulated Au intensity approaches zero under these conditions. Also, just increasing the Au-core diameter while keeping the Ag-shell thickness fixed at the average STEM value would require unrealistic increases in the Au core diameter (>10 nm) for the simulations to match the experimental XPS results. Thus, variation of the Ag shell thickness had a significantly larger effect on simulated Au intensities than changes in the Au-core diameter. This confirms that the Ag-shell thickness of the NPs was effectively thinner than the average value determined from analysis of the STEM images, resulting in stronger experimental XPS Au signals. The no-wash sample also showed the same effects of requiring a thinner Ag shell to match the simulated and experimental Au concentrations.

As discussed above, both NP non-sphericity and off-centered Au-core can contribute to the mismatch between the SESSA and the XPS Au intensities by reducing the effective Ag-shell thickness. Thus, additional simulations were done to account for the effective Ag-shell thickness by incorporating the STEM measured Ag-shell thickness distribution into the SESSA calculations (Figure 6a). Simulations using fixed Au-core dimension and normalizing to the Ag-shell thicknesses based on the STEM measured Ag-shell thickness distribution can deliver the most reliable simulation result by taking considerations of both non-sphericity and off-centered Au-cores. To probe the individual contributions of each to reducing effective Ag-shell thickness, experimentally determined NP non-sphericities and the off-centered Au-core distances were used to reconstruct Ag-shell thickness distributions. To achieve this, the non-sphericity distribution measured quantitatively in Figure 1d was applied to reconstruct the Ag-shell thickness distribution for the Au/Ag-core shell NPs (Figure 6b). Similarly, the distribution of off-centered Au-core distances measured quantitative in Figure 4 was used to generate corresponding Ag-shell thickness distributions (Figure 6c). These normalized Ag-shell thickness distributions represent the specific contribution of non-spherical particles and off-centered Au-cores. In particular, the Ag-shell thicknesses generated from the off-centered Au-core measurements were on average thinner with a wider distribution than compared to the non-sphericity normalized Ag-shell thicknesses.

Although SESSA cannot directly simulate NP samples with a distribution of dimensions, it is possible to simulate various Ag-shell thickness separately and normalize the result based on the corresponding Ag-shell thickness distribution. Figure 7 compares the simulation results for the one- and two-wash samples based on experimentally measured and various normalized Ag-shell thickness distributions shown in Figure 6. As expected, for all models the SESSA simulations showed good fit to the experimental data for all elements except gold. For the one wash sample (Figure 7a), comparing to the experimental gold composition (0.75 atomic %), the simulation based on the average STEM dimensions significantly underestimated the gold composition (0.07 atomic %). The simulation based on the experimentally measured non-sphericity slightly increased gold composition to 0.09 atomic %, while accounting for the off-centered Au-cores showed a much greater increase in gold composition to 0.36 atomic %. Lastly, simulation based on STEM measured Ag-shell thickness distribution, which includes both non-sphericity and off-centered core effects, generated the best match of the simulated gold composition (0.64 atomic %) to the experimental XPS gold composition (0.75 atomic %). Similar effects were also observed for the two wash sample (Figure 7b) and no-wash sample (data not shown). Thus, accounting for the polydispersity of the both non-sphericity and off-centered core for the Au/Ag-core/shell NPs is necessary to obtain good agreement between the SESSA and experimental XPS results, with the off-centered Au-core having a larger effect than the NP non-sphericity.

Conclusions

The new version of spectral modeling software SESSA (Ver. 2.0) was applied to simulate Au/Ag-core/shell NPs that are polydispersed, non-spherical, and contained off-centered Au-cores. The SESSA approach is relatively easy to apply and can provide important information about coatings, coating stability, and the effectiveness of cleaning and other

sample handling processes. The simulation of an “average” ideal spherical particles provided consistent determination of the adventitious hydrocarbon contamination and citrate layer thicknesses, but variations in particle geometry needed to be considered to explain and properly quantify the deviation in the Au signals from the NP core.

Simulation results based on average NP dimensions determined that the Au/Ag-core shell NPs after one and two wash cycles were stabilized with a 0.8 nm thick layer of sodium citrate and coated by a 0.05 nm (one wash) and 0.025 nm (two wash) thick adventitious hydrocarbon overlayers. There was little difference between the samples identified as one and two wash. However, significant differences were observed for the zero and three wash samples, providing information about the durability of the citrate layer to this washing method and the effectiveness of the wash.

Simulating NPs with average dimensions and not accounting for the geometrical properties of the NPs resulted in significant underestimation of the gold intensity. To address this, a series of simulations based on detailed STEM image analysis were performed to include the contribution of the non-ideal geometrical properties. We were able to separate the contribution of NP non-sphericity and off-centered Au-cores and determine their individual impact on the simulated elemental composition of the Au/Ag-core shell NPs. Simulations based on the combined effect of NP non-sphericity and off-centered Au-core resulted in reduced effective Ag-shell thickness and provided simulated elemental compositions that matched the experimental XPS results.

This work demonstrates the impact of using SESSA to model NPs with non-ideal geometrical properties and highlights the benefits of a complementary, multi-technique approach with SESSA, XPS and STEM to obtain a detailed understanding and insight into how to quantify the effects of non-ideal geometries for characterizing the structure and composition of actual NPs. STEM provides dimensional information about the metallic cores and shells that is used to guide selection and establish boundary conditions for the SESSA models, XPS provides information about organic species and contaminants that are difficult to detect or damaged by STEM, and SESSA allows the experimental XPS composition to be converted to quantitative core diameter and shell thickness values. Together they provide more detail about NP structure than could be obtained by using any one of these techniques individually. For the NPs investigated in this study not properly accounting for the non-sphericity and off-set cores in the XPS analysis resulted in a ~50% error in the Au core diameter and a ~25% error in the Ag shell thickness.

Materials and Methods

Materials

The citrate-stabilized Au/Ag-core/shell nanoparticles ~20 nm in diameter used in this study are associated with a National Institute of Environmental Health Sciences (NIEHS) Centers for Nanotechnology Health Implications Research (NCNHIR) consortium examining the toxicology of nanoparticles. The ~20 nm particles had been grown on 7 to 8 nm Au seed particles that were purchased from NanoComposix (San Diego, CA) for consortium use. The as received particles, 1 mg/ml particles suspended in a ~2 mM citrate buffer solution and

packaged in 30 ml plastic containers, were stored in a refrigerator at 4°C before any further processing. As measured by dynamic light scattering, the size of the particles used in this study had remained stable during storage since their arrival at PNNL in November 2011 (longer than the recommended particle shelf lifetime). Papers describing and using these particles in toxicological studies have been published.^{3, 7, 34–36}

Scanning transmission electron microscopy (STEM)

Structural features of the nanoparticles have been analyzed using STEM and high resolution TEM (HR-TEM) imaging and described in an earlier publication.⁷ For STEM imaging in this study a FEI-Titan 80–300 microscope equipped with a probe-forming lens corrector was used and operated at an accelerating voltage of 300 keV. The high-angle annular dark-field (HAADF) image collection angle was 50–200 mrad. STEM samples were prepared by drop casting a drop of suspension onto a 200 mesh lacey carbon TEM grid. STEM data in this paper, as described below, was collected during the course of a previously reported study⁷ that used the same batch of these NPs.

ImageJ software was used to analyze the diameter, non-sphericity, Au-core diameter, Ag-shell thickness, and the degree of the off-centered Au-core of the Au/Ag-core shell NPs. The NP diameters and non-sphericity were determined using the software's particle analysis algorithm. The boundary of the core and shell were determined visually and applied to calculate the Au-core diameter and Ag-shell thickness by measuring the distance of eight radially spaced straight lines originating from the center of the Au-core to the outer edge of the Ag-shell. The degree of the off centered Au-core was determined by calculating the distance between each particle's maxima (center of the Au-core) and ultimate point (center of the whole particle).

X-ray photoelectron spectroscopy (XPS)

XPS measurements were performed with a Physical Electronics Quantera Scanning X-ray Microprobe. This system uses a focused monochromatic Al K α X-ray (1486.7 eV) source for excitation and a spherical section analyzer. The instrument has a 32 element multichannel detection system. A 40 W X-ray beam focused to 200 μ m diameter was used for this analysis. The binding energy (BE) scale is calibrated using the Cu2p $_{3/2}$ peak at 932.62 ± 0.05 eV and Au 4f $_{7/2}$ peak at 83.96 ± 0.05 eV for known reference foils. The X-ray beam is incident normal to the sample and the photoelectron detector is at 45° off-normal. High-energy resolution spectra were collected using a pass-energy of 69.0 eV with a step size of 0.125 eV. For the Ag 3d $_{5/2}$ line, these conditions produced a FWHM of 0.93 eV.

Particles were prepared for XPS analysis by a centrifuge washing process. Stock solution (0.2 mL) was first dispersed in 1.5 ml centrifuge tubes, and then ultra-centrifuged at 30,000 rpm (49,000 \times g maximum, 38,000 \times g average, and 27,000 \times g minimum) for 90 minutes. After the first centrifugation, the supernatant was pipetted off and the particles re-dispersed in 0.2 mL of deionized (DI) water. This re-dispersion was followed by another round of centrifugation and removal of the supernatant. The particles were again re-dispersed and another round of centrifugation followed. After each round of centrifugation a sample of the NPs was saved for XPS analysis. In each case the supernatant was poured off and 20 μ L of

DI water was added to the NP “plug” to assist deposition onto a cleaned Si wafer for XPS analysis. Multiple drops of solution were applied to create a deposit covering the substrate. The material deposited after one centrifugation cycle is labeled ‘one wash’, the sample after two centrifugation cycles is labeled ‘two wash’. Examining particles after one- and two-wash cycles provides some information regarding stability of the citrate coating with regard to the washing process. Both XPS survey and high-energy resolution spectra were acquired from the deposited NPs. High-resolution spectra were collected from the Ag3d, Au4f, C1s, O1s and Na1s regions. The XPS compositional results were calculated using the standard sensitivity factors provided by PHI MultiPak software version 9.5.1.0 using peak area intensities after a Shirley background subtraction.

Simulation of Electron Spectra for Surface Analysis (SESSA) simulation of Au/Ag-core shell NPs

SESSA (Version 2.0) can generate XPS data based on a user-defined layered spherical model.³² The instrumentation parameters used in SESSA including the x-ray source, analyzer, and aperture geometry were set to match the parameters of the PHI Quantera. The properties of the layers such as composition, thickness, and density can be varied to match the experimental XPS results. The density of the layers were estimated by SESSA and assumed to be constant. To determine the elemental composition of the simulated spectra, the peak areas generated by SESSA were divided by their corresponding sensitivity factor and normalized as percent elemental composition. In this work, simulations were done for a single NP as previous studies have shown a single NP provides a good representation of a disordered, powder-like film of NPs.^{11, 32} Lastly, all simulations included elastic scattering of the photoelectrons.

Supplementary Material

Refer to Web version on PubMed Central for supplementary material.

Acknowledgments

Y.-C. Wang and D.G. Castner gratefully acknowledge the support from National Institutes of Health grant EB-002027 to NESAC/BIO from the National Institute of Biomedical Imaging and Bioengineering. D.R. Baer acknowledges support from the National Institutes of Health, National Institute of Environmental Health Sciences (NIEHS) under grant U19 ES019544. The silver nanomaterials were provided by the NIEHS Centers for Nanotechnology Health Implications Research (NCNHIR) Consortium. Y.-C. Wang was supported by the National Science Foundation Graduate Research Fellowship Program under Grant No. DGE-1256082. Any opinions, findings, and conclusions or recommendations expressed in this material are those of the author(s) and do not necessarily reflect the views of the National Science Foundation. A portion of this research was performed at the Environmental Molecular Sciences Laboratory (EMSL), a national scientific user facility sponsored by the DOE’s Office of Biological and Environmental Research and is located at Pacific Northwest National Laboratory (PNNL). We thank Drs. J. Smith and P. Musuamy for assistance with preparation of the samples for the XPS measurements and Dr. C. Wang for the STEM measurements that were reported in ¹⁰. We thank M. Chudzicki, C. Powell, A. Shard, and W. Werner for stimulating discussions regarding XPS analysis of nanoparticles.

References

1. Belsey NA, Shard AG, Minelli C. *Biointerphases*. 2015; 10:019012. [PubMed: 25724220]
2. Grainger DW, Castner DG. *Advanced Materials*. 2008; 20:867–877.

3. Baer DR, Engelhard MH, Johnson GE, Laskin J, Lai J, Mueller K, Munusamy P, Thevuthasan S, Wang H, Washton N, Elder A, Baisch BL, Karakoti A, Kuchibhatla SV, Moon D. *J Phys Chem A*. 2013; 31:050820.
4. Baer DR, Gaspar DJ, Nachimuthu P, Techane SD, Castner DG. *Anal Bioanal Chem*. 2010; 396:983–1002. [PubMed: 20052578]
5. Nel AE, Parak WJ, Chan WCW, Xia T, Hersam MC, Brinker JC, Zink JI, Pinkerton KE, Baer DR, Weiss PS. *ACS Nano*. 2015; 9:5627–5630. [PubMed: 26100220]
6. Unfried K, Albrecht C, Klotz LO, Mikecz VA. *Nanotoxicology*. 2007; 1:52–71.
7. Munusamy P, Wang C, Engelhard MH, Baer DR. *Biointerphases*. 2015
8. Murphy CJ, Gole AM, Stone JW, Sisco PN. *Acc Chem Res*. 2008; 41:1721–1730. [PubMed: 18712884]
9. Jiang W, Kim BYS, Rutka JT, Chan WCW. *Nat Nanotechnol*. 2008; 3:145–150. [PubMed: 18654486]
10. Hassellöv M, Readman JW, Ranville JF, Tiede K. *Ecotoxicology*. 2008; 17:344–361. [PubMed: 18483764]
11. Frydman A, Castner DG, Schmal M, Campbell CT. *J Catal*. 1995; 157:133–144.
12. Techane S, Baer DR, Castner DG. *Anal Chem*. 2011; 83:6704–6712. [PubMed: 21744862]
13. Zorn G, Dave SR, Gao X, Castner DG. *Anal Chem*. 2011; 83:866–873. [PubMed: 21226467]
14. Zorn G, Dave SR, Weidner T, Gao X, Castner DG. *Surf Sci*. 2016; 648:339–344. [PubMed: 26924858]
15. Bell NC, Minelli C, Shard AG. *Anal Methods*. 2013; 5:4591–4601.
16. Pourcelle V, Devouge S, Garinot M, Pr eat V. *Biomacromolecules*. 2007; 8:3977–3983. [PubMed: 18039005]
17. Shenoy DB, Amiji MM. *Int J Pharmaceutics*. 2005; 293:261–270.
18. Techane SD, Gamble LJ. *J Phys Chem C*. 2011; 115:9432–9441.
19. Techane SD, Gamble LJ, Castner DG. *Biointerphases*. 2011; 6:98–104. [PubMed: 21974680]
20. Torelli MD, Putans RA, Tan Y, Lohse SE. *ACS Appl Mater Interfaces*. 2015; 7:1720–1725. [PubMed: 25514372]
21. Yang HM, Park CW, Woo MA, Kim MI, Jo YM. *Biomacromolecules*. 2010; 11:2866–2872. [PubMed: 20932000]
22. Gillet JN, Meunier M. *J Phys Chem: B*. 2005; 109:8733–8737. [PubMed: 16852034]
23. Yang DQ, Gillet JN, Meunier M. *J Appl Phys*. 2005; 97:024303.
24. Shard AG. *J Phys Chem C*. 2012:16806–16813.
25. Cant DJH, Wang Y-C, Castner DG, Shard AG. *Surf Interface Anal*. 2016; 48 in press.
26. Mohai M. *Surf Interface Anal*. 2004:828–832.
27. Mohai M, Bertoti I. *Surf Interface Anal*. 2004; 36:805–808.
28. Tougaard S. *J Phys Chem A*. 1996; 14:1415–1423.
29. Tougaard, S. Software packages to characterize surface nano-structures by analysis of electron spectra. 2012.
30. Werner, SMW.; WS; Powell, JC. NIST Database for the Simulation of Electron Spectra for Surface Analysis (SESSA): Version 2.0. National Institute of Standards and Technology; Gaithersburg, MD: 2015.
31. Smekal W, Werner WSM, Powell CJ. *Surf Interface Anal*. 2005; 37:1059–1067.
32. Werner W, Chudzicki M, Smekal W, Powell CJ. *Appl Phys Lett*. 2014; 104:243106.
33. Chudzicki M, Werner W, Shard AG, Wang YC, Castner DG, Powell CJ. *J Phys Chem C*. 2015; 119:17687–17696.
34. Holland BN, Shannahan JH. *Journal of Nanomedicine & Nanotechnology*. 2015:s6.
35. Shannahan JH, Lai X, Ke PC, Podila R, Brown JM. *PLoS One*. 2013; 8:e74001. [PubMed: 24040142]
36. Wang X, Ji Z, Chang CH, Zhang H, Wang M, Liao YP, Lin S, Meng H, Li R, Sun B, Winkle LV, Pinkerton KE, Zink JI, Xia T, Nel AE. *Small*. 2014; 10:385–398. [PubMed: 24039004]

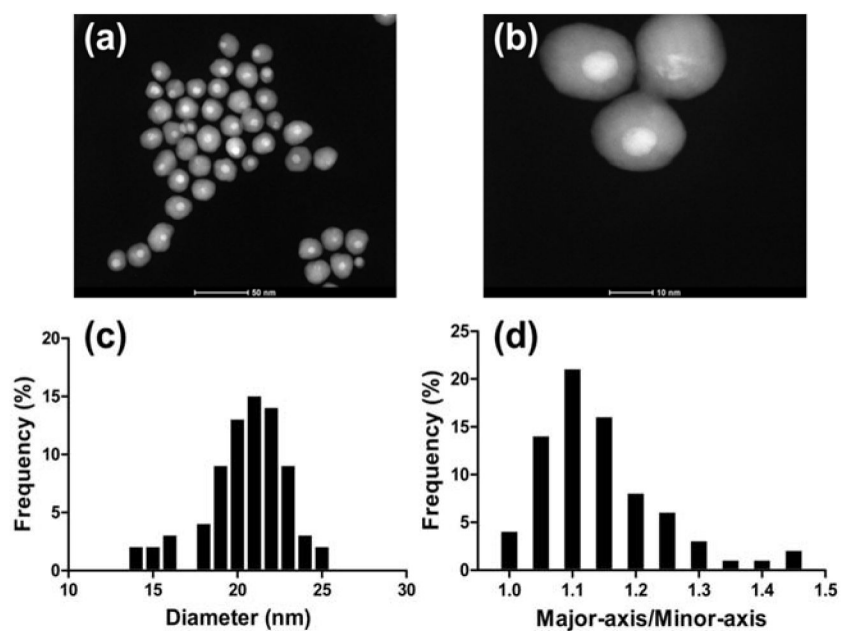


Figure 1. (a & b) STEM images of Au/Ag-core/shell nanoparticles. (c) Distribution of Au/Ag-core/shell nanoparticle diameter with a bin width of 1 nm and a mean diameter of 20.5 ± 2.4 nm ($n = 76$ particles). (d) Distribution of Au-core Ag shell nanoparticle major-axis/minor-axis ratio with a bin width of 0.05 and a mean ratio of 1.14 ± 0.1 ($n = 76$ particles).



Figure 2. Cross sectional schematic of an average, ideal Au/Ag core/shell nanoparticle. The mean for the measured Au-core diameter and Ag-shell thickness was 7.4 ± 0.9 nm and 6.4 ± 2.3 nm (52 particles), respectively. Whole particle diameter derived from the manually measured mean core diameter and shell thickness (20.2 nm) matches closely to the whole particle diameter measured using ImageJ's particle analysis algorithm (20.5 ± 2.4 nm). Figure not to scale.

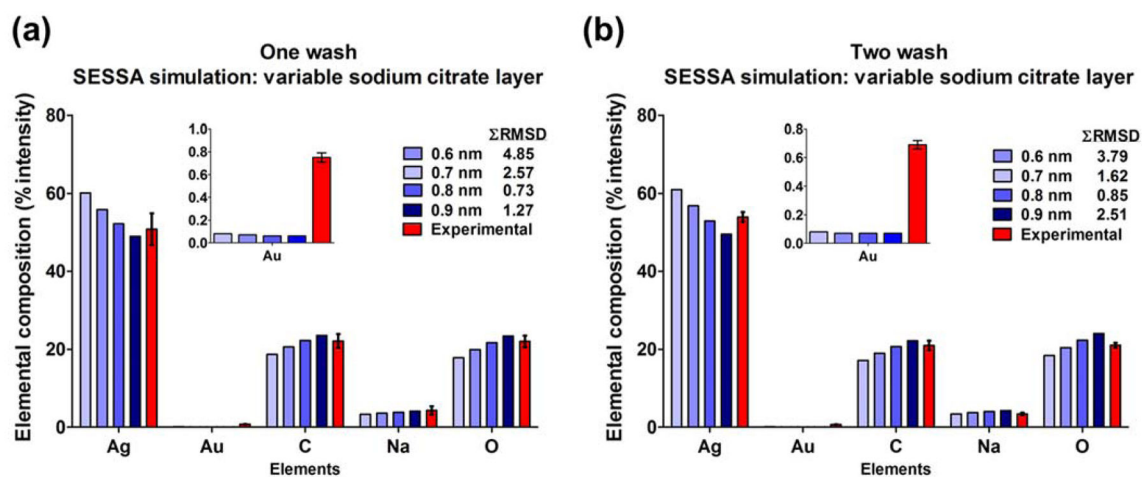


Figure 3.

Comparison of experimental XPS result and SESSA simulation of the composition for Au/Ag-core/shell nanoparticles with varying sodium citrate thickness ranging from 0.6 nm to 1.0 nm for the one-wash (a) and two-wash (b) samples. The sum root mean square deviation (Σ RMSD) indicates the simulated elemental composition (%) for all elements compared to the experimental XPS result.

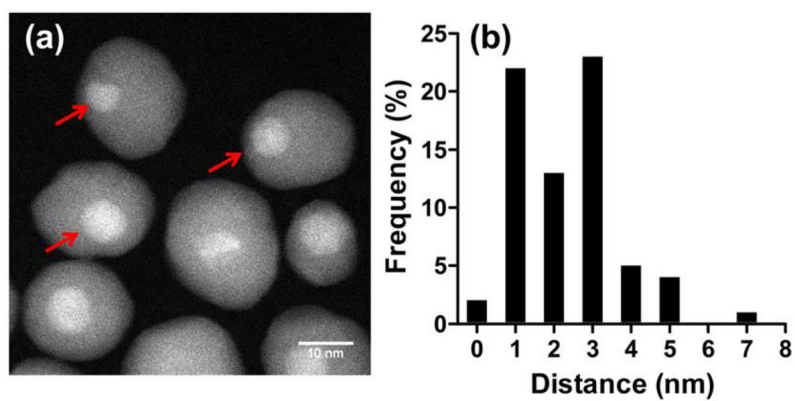


Figure 4. (a) STEM images of Au/Ag-core/shell nanoparticles containing non-centered cores as highlighted by red arrows. (b) Distribution of the distance of gold core off-center relative to the whole Au/Ag-core/shell nanoparticle with bin width of 1 nm and mean distance of 2.2 ± 1.3 nm ($n = 70$ particles).

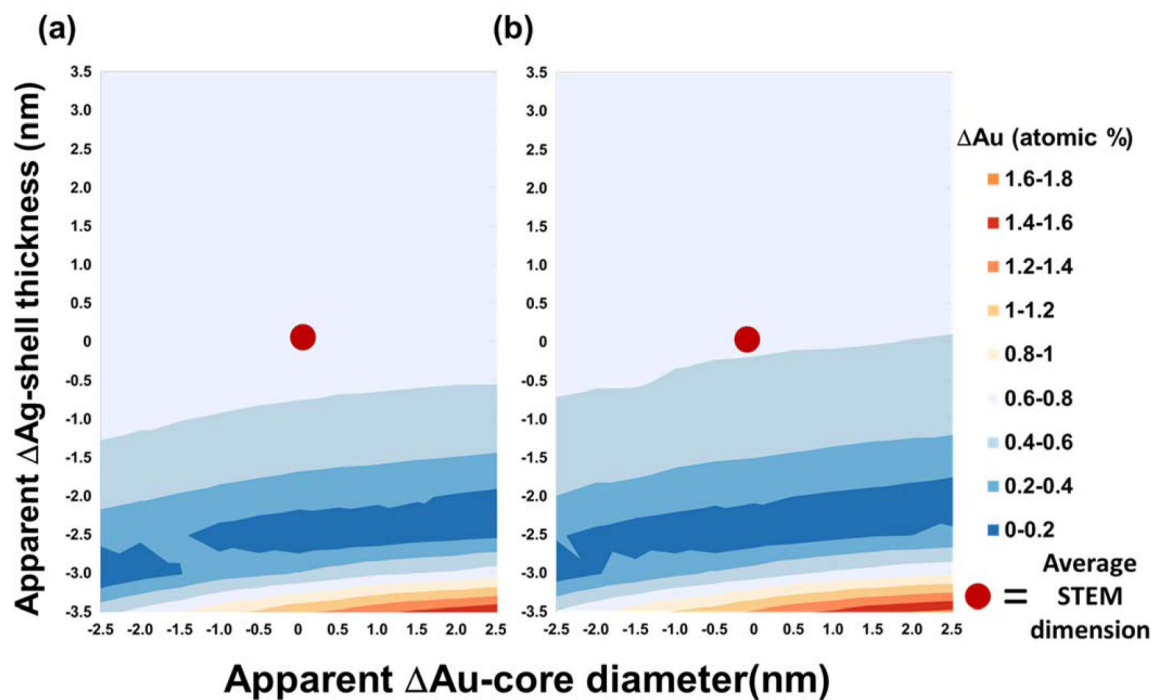


Figure 5. Comparison of experimental XPS and SESSA simulated Au atomic % for varying Ag-shell thicknesses and Au-core diameters. The apparent Ag-shell thickness and Au-core thickness are relative to the average particle dimensions. (a) One centrifuge wash. (b) Two centrifuge washes. The red dot on both panels indicates the average dimensions of the Au-core and Ag-shell determined by STEM.

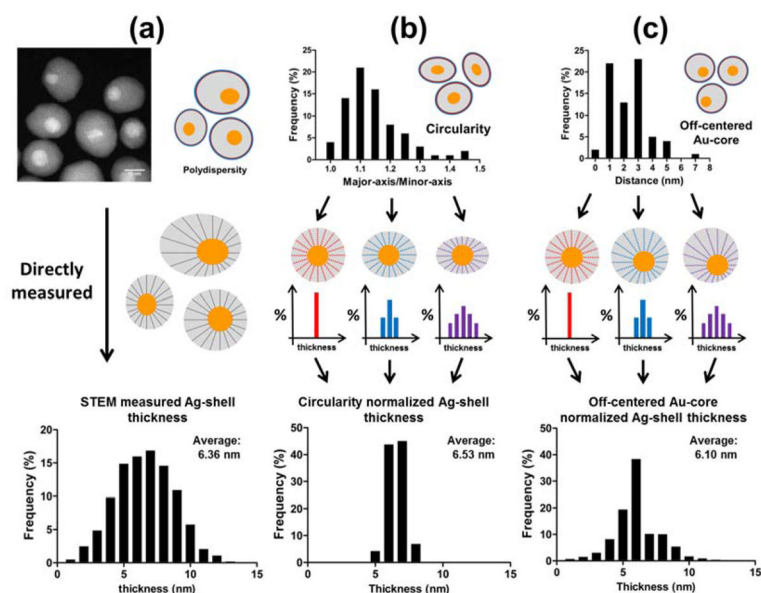


Figure 6. Schematic illustration of the Ag-shell thickness normalization using: (a) the experimentally measured Ag-shell thickness distribution from STEM analysis, (b) only the non-sphericity of the Au/Ag-core shell NPs and assuming the Au-core is located in the center of the particle, and (c) only the degree of off-centered for the Au-core while assuming the particle is perfectly spherical.

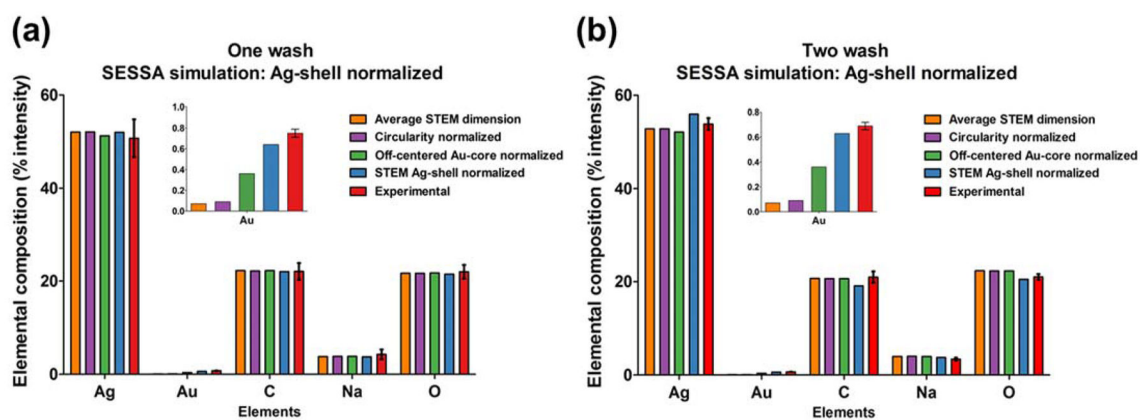


Figure 7. Comparison of experimental XPS results and SESSA simulations for the (a) one-wash and (b) two-wash Au/Ag-core/shell NPs based on the average STEM dimension, non-sphericity normalized, off-centered Au-core normalized, and the STEM Ag-shell normalized Ag-shell thickness distribution. By including the impacts of both non-sphericity and off-center cores based on the STEM distributions, the model matches the experimental data and the off-centered cores were found to have the greatest impact.

XPS determined atomic composition of Au/Ag core-shell nanoparticles deposited onto silicon wafer substrates. Average values and standard deviations are reported for six replicate analyses of the one- and two-wash samples. Only one analysis is reported for the no-wash sample (see text for details).

Table 1

Sample	XPS Atomic Percent				
	Silver	Gold	Carbon	Oxygen	Sodium
no wash (n = 1)	26.1	0.41	40.3	29.0	4.2
one wash (n = 6)	50.9 ± 4.1	0.75 ± 0.04	22.1 ± 1.8	22.0 ± 1.5	4.3 ± 1.1
two wash (n = 6)	53.9 ± 1.3	0.69 ± 0.03	21.0 ± 1.2	21.0 ± 0.6	3.4 ± 0.3